



**HAL**  
open science

## Comparative studies of new pyranilidene-based sensitizers bearing single or double anchoring groups for dye-sensitized solar cells

Sebastien Gauthier, Françoise Robin-Le Guen, Laurianne Wojcik, Nicolas Le Poul, Aurélien Planchat, Yann Pellegrin, Patricia Guevara Level, Nadine Szuwarski, Mohammed Boujtita, Denis Jacquemin, et al.

### ► To cite this version:

Sebastien Gauthier, Françoise Robin-Le Guen, Laurianne Wojcik, Nicolas Le Poul, Aurélien Planchat, et al.. Comparative studies of new pyranilidene-based sensitizers bearing single or double anchoring groups for dye-sensitized solar cells. *Solar Energy*, 2020, 205, pp.310-319. 10.1016/j.solener.2020.05.036 . hal-02873424

**HAL Id: hal-02873424**

**<https://hal.univ-brest.fr/hal-02873424>**

Submitted on 25 Nov 2020

**HAL** is a multi-disciplinary open access archive for the deposit and dissemination of scientific research documents, whether they are published or not. The documents may come from teaching and research institutions in France or abroad, or from public or private research centers.

L'archive ouverte pluridisciplinaire **HAL**, est destinée au dépôt et à la diffusion de documents scientifiques de niveau recherche, publiés ou non, émanant des établissements d'enseignement et de recherche français ou étrangers, des laboratoires publics ou privés.

# **Comparative Studies of New Pyranylidene-Based Sensitizers Bearing Single or Double Anchoring Groups for Dye-Sensitized Solar Cells**

Sébastien Gauthier,<sup>a,\*</sup> Françoise Robin-Le Guen,<sup>a</sup> Laurianne Wojcik,<sup>b</sup> Nicolas Le Poul,<sup>b</sup>

Aurélien Planchat,<sup>c</sup> Yann Pellegrin,<sup>c\*</sup> Patricia Guevara Level,<sup>c</sup> Nadine Szuwarski,<sup>c</sup>

Mohammed Boujtita,<sup>c</sup> Denis Jacquemin<sup>c,\*</sup> and Fabrice Odobel<sup>c,\*</sup>

<sup>a</sup> Univ. Rennes, CNRS, ISCR (Institut des Sciences Chimiques de Rennes) - UMR 6226, F-35000 Rennes, France. E-mail: sebastien.gauthier@univ-rennes1.fr, Tel: +33 2 96 46 93 44.

<sup>b</sup> Laboratoire de Chimie, Électrochimie Moléculaires et Chimie Analytique, UMR CNRS 6521, Université de Bretagne Occidentale, UFR Sciences et Techniques, 6 avenue Victor Le Gorgeu – CS 93837, F-29238 Brest Cedex 3, France.

<sup>c</sup> Université de Nantes, CNRS, CEISAM UMR 6230, F-44000 Nantes, France. E-mails & Tels: yann.pellegrin@univ-nantes.fr, +33 2 76 64 51 74; denis.jacquemin@univ-nantes.fr, +33 2 51 12 55 67; fabrice.odobel@univ-nantes.fr, +33 2 51 12 54 29.

## Abstract

Mono- and di-anchoring  $\gamma$ -pyranylidene-based organic dyes featuring D- $\pi$ -A and D-( $\pi$ -A)<sub>2</sub> architectures have been engineered as sensitizers for applications in Dye-Sensitized Solar Cells (DSSCs). Their photophysical, electrochemical and photovoltaic properties were further investigated. TD-DFT calculations were performed to rationalize the trends observed in the optical and electrochemical properties of the dyes. The investigation of the photovoltaic performances of this series of new dyes provided structure-property relationships where their Power Conversion Efficiencies (PCE) could be correlated to structural features, such as the length of the  $\pi$ -conjugated spacer, the nature of the substituents on the pyranylidene electron donor moiety and the number of anchoring groups. Dye-Sensitized Solar Cells based on mono-anchoring dyes were more efficient than the corresponding cells based on di-anchoring analogues due to high dye loading. The highest Power Conversion Efficiency of 5.23% was achieved with the mono-anchoring **17a** dye containing *t*-butyl substituent groups on the pyranylidene fragment and with one thienyl  $\pi$ -conjugated spacer.

## Keywords

- Dye-sensitized solar cells
- $\gamma$ -pyranylidene
- Substituent effect
- Single and double anchoring dyes
- Photovoltaic performance
- TD-DFT calculations

## 1. Introduction

The development and implementation of renewable energy sources with low carbon emissions have become a paramount environmental requirement to reduce the massive use of fossil fuels. Harvesting the solar power is an attractive, environmentally friendly and renewable energy source, since the sun provides the earth with an energy power about 4000 times the current forecast energy needs of the whole humanity in 2050 (Bandara et al., 2010; Hagfeldt et al., 2010; Hsu et al., 2014; Lewis and Nocera, 2006). Photovoltaic devices, such as solar cells, are certainly the most valuable artificial systems able to directly convert light energy into electricity, and have been the subject of increased research efforts for their development and optimization over the past few years (Imahori et al., 2009; H.-P. Wu et al., 2012; Wu and Zhu, 2013).

Among them, Dye-Sensitized Solar Cells (DSSCs) have emerged as a promising and competitive technology with sizeable Power Conversion Efficiency (PCE) and facile device fabrication, as demonstrated in the seminal work of O'Regan and Grätzel in 1991 (Higashino and Imahori, 2015; O'Regan and Grätzel, 1991). DSSCs consisting of a dyed wide-band gap n-type metal oxide semiconductor such as  $\text{TiO}_2$  as photoanode, a Pt counter-electrode and a redox electrolyte, operate through a process whereby the energy of the absorbed sunlight is transferred from the anchored dye to the acceptor metal oxide semiconductor (Grätzel, 2009). In their original work, O'Regan and Grätzel used ruthenium-based photosensitizers as dyes in their DSSCs. In recent years, research efforts have been devoted to eliminate the need for expensive metals and have focused on the development of metal-free organic dye sensitizers, usually based on push-pull type donor-(spacer)-acceptor (D- $\pi$ -A) molecular structures (Mishra et al., 2009; Ooyama and Harima, 2012; Qu et al., 2012; Y. Wu et al., 2012). In addition to their affordability, these D- $\pi$ -A molecular systems present several advantages, such as their simple preparation process, their easily adjustable structures, their high molar

extinction coefficients and their excellent intra-molecular charge transfer (ICT) photoexcitation properties (Bessho et al., 2010; Mao et al., 2012; Marszalek et al., 2013). In order to enhance the Power Conversion Efficiency (PCE) of D- $\pi$ -A dyes, multiple modifications have been performed on these molecular systems that consisted of varying the donor, spacer, and acceptor moieties (Cai et al., 2013; Choi et al., 2008; Ji et al., 2018; Yao et al., 2015). Numerous metal-free organic dyes containing conjugated electron-donor groups, such as triphenylamine (Wang et al., 2016), dialkylaminophenyl (Liang and Chen, 2013), indoline (Alagumalai et al., 2016; Yang et al., 2014), carbazole (Sathiyam et al., 2016; Soni et al., 2015), dithiafulvene (Luo et al., 2016; Wan et al., 2014) and tetrathiafulvalene (TTF) (Brunetti et al., 2012; Wenger et al., 2010) groups have been successfully used as sensitizers in DSSCs, the most efficient exhibiting PCE reaching up to 12%. It has been reported that the PCE performances of DSSCs can be enhanced by extending the  $\pi$ -conjugation of the dyes, increasing the strength of the donor/acceptor units and improving the adsorption of the dyes onto the TiO<sub>2</sub> surface (Yeh-Yung Lin et al., 2014). Due to the importance of the anchoring group on the binding energy of the dye onto TiO<sub>2</sub> and the electron injection rate, selecting an appropriate anchoring moiety is particularly crucial for enhancing the device's performance. In the majority of organic dyes, carboxylic or cyanoacrylic acids are used as they play the dual role of electron acceptor and anchoring site to tether the dye molecules onto the TiO<sub>2</sub> surface (Zhang and Cole, 2015). The strong bonding of the carboxylic acid group onto the TiO<sub>2</sub> surface allows for a good electronic coupling between the dye and TiO<sub>2</sub>, thus providing a high electron injection rate (Ambrosio et al., 2012; Srinivas et al., 2009; Wiberg et al., 2009).

Improving light-absorbing capability, suppressing charge recombination, increasing electron extraction channels and enhancing the binding strength with the semiconductor surface are important factors for improving the overall performance of DSSCs. These requirements can

be, at least partially, met by incorporating two or more anchoring groups in the dye molecular structures (Abbotto et al., 2009; Grisorio et al., 2013; Gupta et al., 2014; Zhang et al., 2013). Indeed, DSSCs organic dyes synthesized with several anchoring groups were recently reported to display enhanced photovoltaic properties compared to their counterparts containing only one binding group (Berhe Desta et al., 2017; Jia et al., 2016; Li et al., 2017).  $\gamma$ -Pyranlydene fragments have been incorporated as electron-donating groups in organic molecules and in various platinum- and ruthenium-based organometallic complexes for the preparation of push-pull chromophores for second-order Non-Linear Optics (NLO) (Durand et al., 2018, 2017; Gauthier et al., 2018, 2013; Marco et al., 2015, 2013) and/or DSSCs (Andreu et al., 2009; Bolag et al., 2012; Ferreira et al., 2017; Gauthier et al., 2014). Various  $\gamma$ -pyranlydene fragments have been found to be effective donors in D- $\pi$ -A sensitizers for DSSCs yielding promising PCE of up to 6% (Marco et al., 2019). Recently, one di-anchoring D-( $\pi$ -A)<sub>2</sub> type organic dye based on  $\gamma$ -pyranlydene core with two anchoring acceptor groups was designed and synthesized by Franco and co-workers (Andrés-Castán et al., 2019). They found that the Photo Conversion Efficiency of this di-anchoring  $\gamma$ -pyranlydene-based D-( $\pi$ -A)<sub>2</sub> dye was higher than that of the mono-anchoring D- $\pi$ -A analogue due to improved photocurrent and stability.

Despite a demonstrated improvement of the PCE in DSSC systems containing di-anchoring dyes, the development of dyes with multiple anchoring sites has been relatively unexplored so far. To address this shortcoming, we have designed and synthesized a new series of di-anchoring D-( $\pi$ -A)<sub>2</sub> push-pull dyes **10a-c** and **12c**, based on the pyranlydene group (Fig. 1). The photophysical properties of these di-anchoring D-( $\pi$ -A)<sub>2</sub> push-pull dyes have been compared to their mono-anchoring analogues, such as compound **17a** presented in this paper and compounds **D1**, **D2** and **D3** previously investigated in our research group (Fig. 1.) (Gauthier et al., 2019)

Our approach was to investigate the effects of a variety of structural modifications, such as donors with different substituents on the pyranilidene ring (*i.e.* phenyl (**10b**), *t*-butyl (**10a**), thienyl (**10c**)), the nature of the linker (**10c** versus **12c**), the number of anchoring groups (**10a** versus **17a**, **10b** versus **D1**, **10c** versus **D2** and **12c** versus **D3**), and the length of the linker for the dyes with a single anchoring group (*i.e.* one thienyl (**17a**), two thienyl (**18a**), and three thienyl units (**19a**)), on the optical, electrochemical and photovoltaic properties of the dyes. The organic compounds, prepared in this study, were fully characterized by various techniques and their efficiency was evaluated in TiO<sub>2</sub>-based DSSCs. Theoretical studies were also conducted to support the experimental data and to correlate the dye structures to their electronic properties.

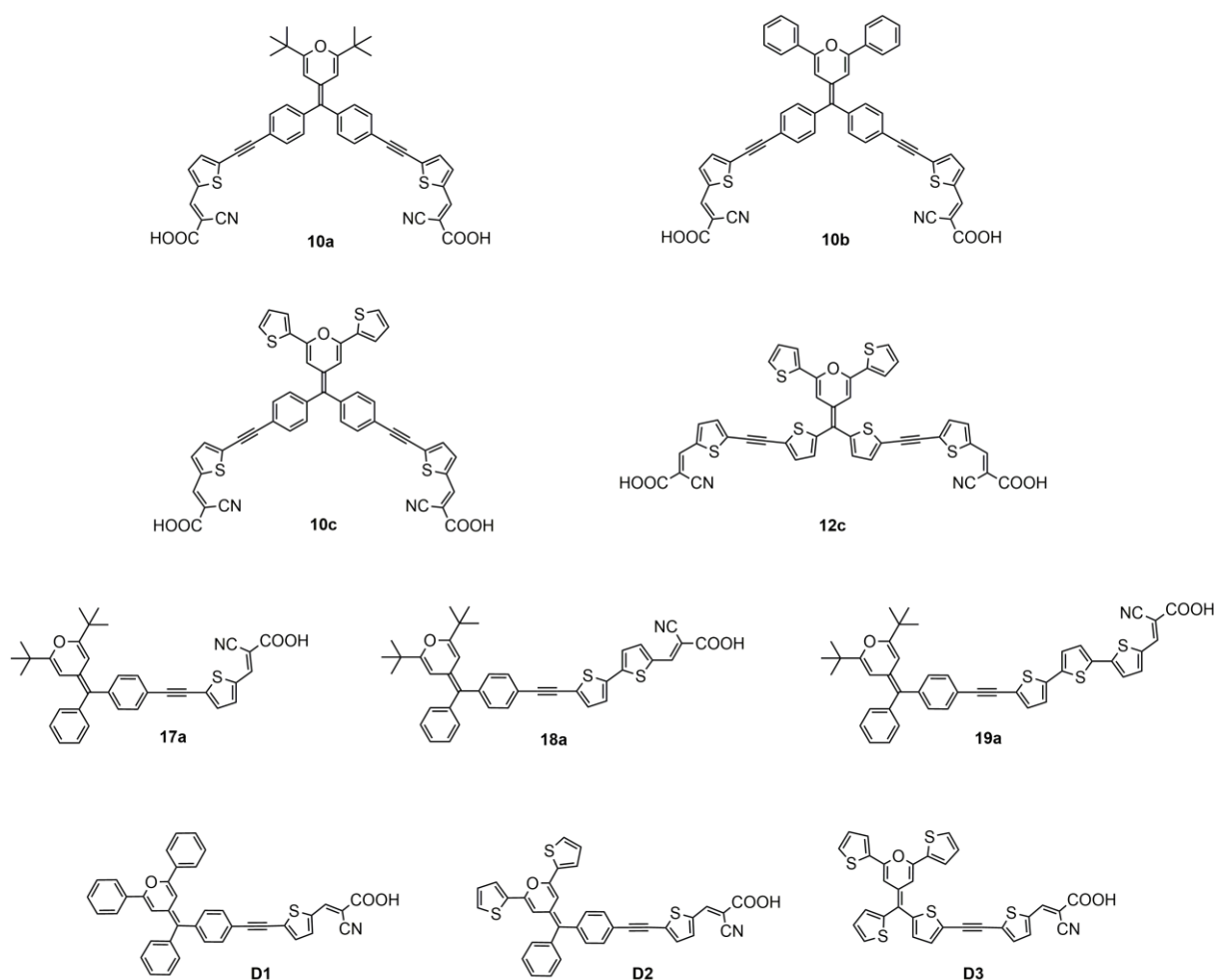
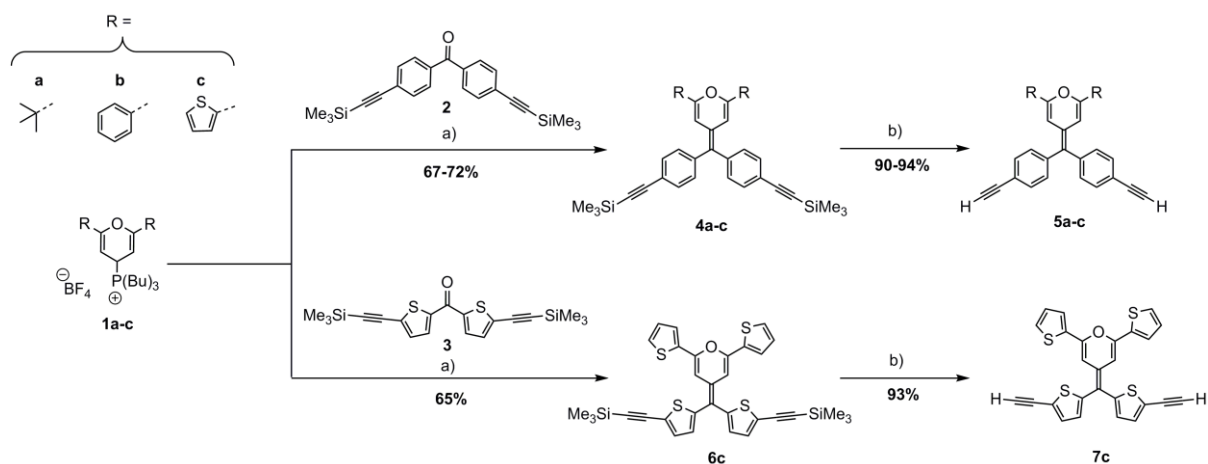


**Fig. 1.** Structures of the dyes investigated in this work (**10a-c**, **12c**, **17a**, **18a**, **19a**) and previously studied (**D1-3**) (Gauthier et al., 2019)

## 2. Results and Discussion

### 2.1. Synthesis of the Dyes

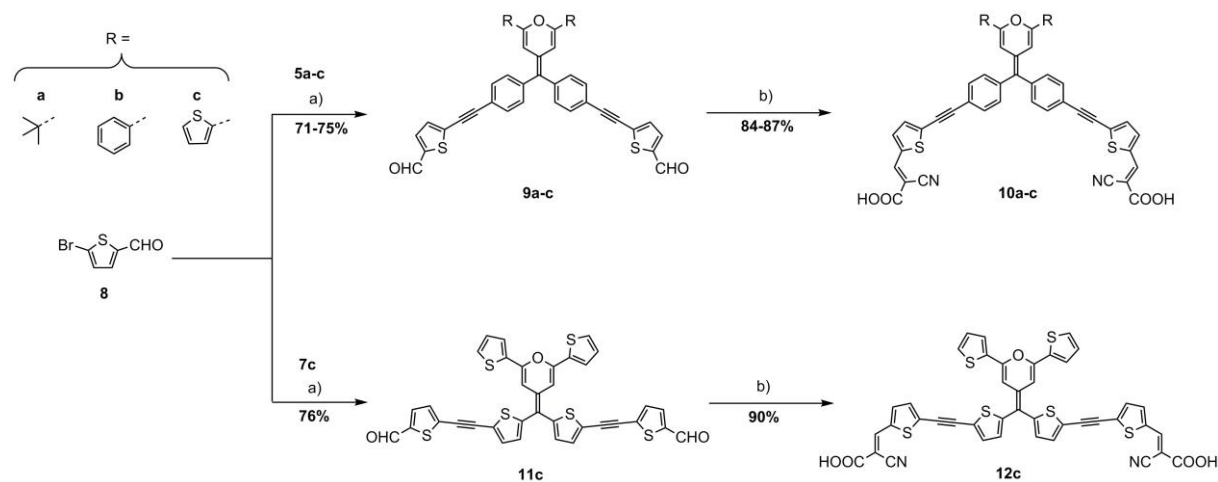
The key intermediate in the preparation of di-anchoring D-( $\pi$ -A)<sub>2</sub> push-pull dyes is the di-alkynes **5a-c** and **7c** (Scheme 1). First, the di-alkyne **5b** is prepared according to previously described synthetic routes (Gauthier et al., 2018). Identical synthetic pathways are used for **5a**, **5b**, and **7c**, which are obtained in two steps from bis[4-(2-trimethylsilylethynyl)]benzophenone **2** or bis[5-(2-trimethylsilylethynyl)]thienone **3** and the desired phosphonium tetrafluoroborate salt **1a-c** (Gauthier et al., 2019, 2014) (Scheme 1). The first step is a Wittig reaction leading to the intermediates **4a-c** and **6c** obtained in good yield, whereas the second step consists of the deprotection of the trimethylsilyl group with quasi-quantitative yield.



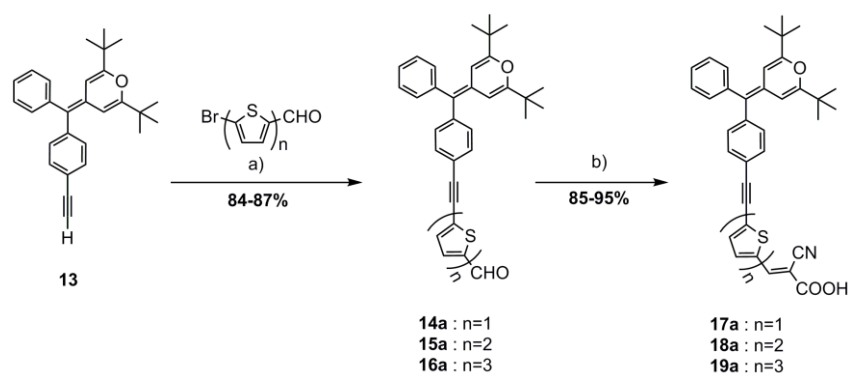
**Scheme 1.** Synthesis of alkyne compounds **5a-c** and **7c**. Reagents and conditions: a) THF, n-BuLi, -78°C to r.t., 2h. b) K<sub>2</sub>CO<sub>3</sub>, CH<sub>2</sub>Cl<sub>2</sub>/MeOH, r.t., overnight.

The mono- and di-carboxaldehyde intermediates **9a-c**, **11c**, **14a**, **15a**, and **16a**, are then obtained from a copper/palladium catalyzed Sonogashira cross-coupling reaction of **5a-c**, **7c** and **13** with the corresponding aldehydes **8** (Scheme 2 and 3). Finally, the dyes **10a-c**, **12c**, **17a**, **18a**, and **19a** are obtained in good yields (84–95%) through Knoevenagel reactions of

the corresponding precursors with cyanoacetic acid in the presence of piperidine and subsequent acid wash (Scheme 2 and 3).



**Scheme 2.** Synthesis of dyes **10a-c** and **12c**. Reagents and conditions: a) Pd(PPh<sub>3</sub>)<sub>4</sub>, CuI, THF, NH*i*Pr<sub>2</sub>, 60° C, overnight. b) Cyanoacetic acid, piperidine, CHCl<sub>3</sub>, reflux, overnight.



**Scheme 3.** Synthesis of dyes **17a**, **18a** and **19a**. Reagents and conditions: a) Pd(PPh<sub>3</sub>)<sub>4</sub>, CuI, THF, NH*i*Pr<sub>2</sub>, 60° C, overnight. b) Cyanoacetic acid, piperidine, CHCl<sub>3</sub>, reflux, overnight.

All targeted sensitizer dyes have been characterized by <sup>1</sup>H and <sup>13</sup>C NMR, and high-resolution mass spectrometry. All the NMR spectra of the new compounds are presented in the Supplementary Information (SI). These new dyes are also perfectly stable in their solid state and do not require any specific storage conditions.

## 2.2. Electronic UV-visible absorption

The electronic spectra of compounds **10a-c**, **12c**, **17a**, **18a**, and **19a** obtained in dichloromethane ( $1.1 \times 10^{-5}$  M) in the 300–800 nm wavelength range are shown in Fig. 2 and the key spectroscopic features are summarized in Table 1. The absorption bands of the dyes can be separated into two groups falling in the regions 300-450 nm and 450-600 nm. For all compounds, the absorption bands in the high-energy region correspond to localized  $\pi$ - $\pi^*$  transitions originating from the pyranilidene-oligothienyl segment, whereas the least energetic absorption bands in the visible region can be assigned to an ICT process between the pyranilidene donor unit to the cyanoacrylic acid acceptor (see theoretical calculations below).

Molar extinction coefficients ( $\epsilon$ ) obtained for compounds **10a-c**, **12c**, **17a**, **18a**, and **19a** are larger than  $23,900 \text{ M}^{-1}\text{cm}^{-1}$  with a maximum at  $50,000 \text{ M}^{-1}\text{cm}^{-1}$  for compound **10a**. These coefficients exceed those of the standard ruthenium dyes N3 (Horiuchi et al., 2003) and N719 (Wang et al., 2005) ( $13,900$  and  $14,000 \text{ M}^{-1}\text{cm}^{-1}$ , respectively), indicating that most of the dyes of this series should be good light harvesting compounds.

The groups placed in the 2- and the 6- positions of the pyranilidene fragment (i.e., phenyl, thienyl, *t*-butyl) have a limited influence on the absorption properties, which is consistent with the topology of the involved excited states (see below). Finally, the potential effects on the absorption properties of the nature of the substituents placed on the exocyclic carbon of the pyranilidene moiety of **10c** and **12c** dyes were examined. While the replacement of a phenyl by a thienyl substituent (**10c** versus **12c**) has a limited influence on the absorption band wavelength, it leads to a significantly lower molar extinction coefficient (the same observation can be made when comparing **D2** to **D3**) (Gauthier et al., 2019). In addition, the main visible absorption of the di-anchoring D-( $\pi$ -A)<sub>2</sub> **10a**, **10b** and **10c** dyes appears at a wavelength similar to that of the mono-anchoring D- $\pi$ -A **17a**, **D1** and **D2** analogues.

However, a significant red-shift ( $\Delta = 15$  nm) is observed when comparing the absorption spectra of the mono-anchoring D- $\pi$ -A **D3** and its di-anchoring D-( $\pi$ -A)<sub>2</sub> **12c** analogue.

The increase of the maximum absorption and the red-shift of the maximum absorption of **19a** compared to that of **18a** can be explained by the enhanced electron delocalization over oligothieryl spacers of increasing lengths. The same phenomenon has been observed for other organic dyes when the  $\pi$ -conjugation of the spacers is extended (Bologan et al., 2012; Fischer et al., 2010).

**Table 1**

Absorption properties of the dyes **10a-c**, **12c**, **17a**, **18a**, **19a**, **D1**, **D2** and **D3** recorded in CH<sub>2</sub>Cl<sub>2</sub> ( $1.1 \times 10^{-5}$  M) at room temperature.

| Dye        | $\lambda_{\max}/\text{nm}$<br>( $\epsilon \times 10^4 \text{ M}^{-1} \cdot \text{cm}^{-1}$ ) | $\lambda_{\text{onset}}/\text{nm}^a$ |
|------------|--|--------------------------------------|
| <b>10a</b> | 396 (5,0), 485 (sh)  | 569                                  |
| <b>10b</b> | 393 (4,8), 480 (sh)  | 556                                  |
| <b>10c</b> | 393 (4,2), 470 (sh)  | 564                                  |
| <b>12c</b> | 391 (2,4), 500 (sh)  | 630                                  |
| <b>17a</b> | 379 (2.7), 472 (1.5)   | 566                                  |
| <b>18a</b> | 442 (4.1)  | 543                                  |
| <b>19a</b> | 366 (sh), 462 (4.8)  | 540                                  |
| <b>D1</b>  | 387 (4.8), 480 (sh)  | 568                                  |
| <b>D2</b>  | 389 (5.3), 472 (sh)  | 568                                  |
| <b>D3</b>  | 406 (3.4), 520 (sh)  | 655                                  |

<sup>a</sup> Estimated from the wavelength with the intersections tangent method ( $\lambda_{\text{onset}}$ ).

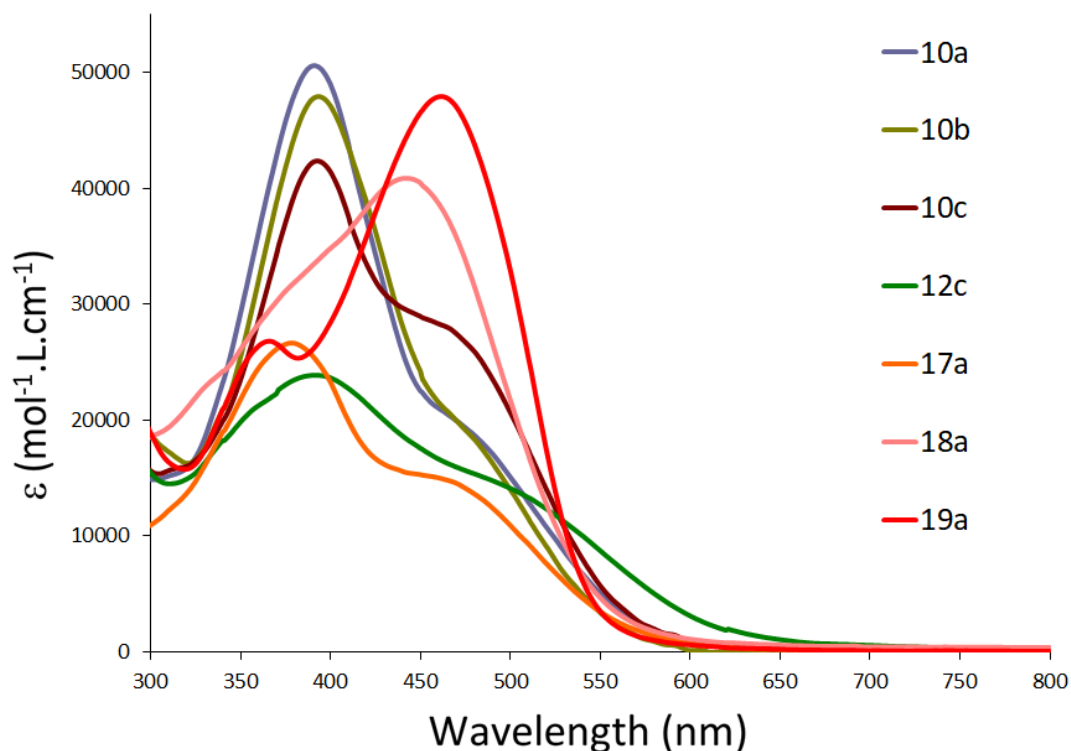


**Fig. 2.** UV-Vis absorption spectra of **10a-c**, **12c**, **17a**, **18a**, and **19a** in  $\text{CH}_2\text{Cl}_2$  solution ( $1.1 \times 10^{-5}$  M) at room temperature.

### 2.3. Electrochemical study and electron transfer driving forces

The redox properties of the dyes were investigated by using cyclic voltammetry (CV). Table 2 presents the electrochemical data obtained from experiments conducted with a platinum working electrode. Redox potential values are measured against ferrocene and recalibrated *versus* NHE. All experiments were carried out in dichloromethane except for compounds **10b**, **10c** and **12c** (in  $\text{CH}_2\text{Cl}_2/\text{THF}$  or THF) because of their low solubility in dichloromethane at the millimolar concentration. Electrochemical data obtained for compound **10a** in both  $\text{CH}_2\text{Cl}_2$  and  $\text{CH}_2\text{Cl}_2/\text{THF}$  indicate that the solvent has a very limited impact on the voltammetry response (see Table 2).

All pyranylidenes display similar voltammetric signatures, *i.e.*, two successive oxidation processes (excluded compound **17a** which shows only one), and one (or two) broad reduction peaks starting from the open-circuit potential. This redox behavior is reminiscent of those observed with analogous compounds such as **D1-D3** (Durand et al., 2017; Gauthier et al., 2014, 2019). Fig. 3A shows CVs for both compounds **10a** and **17a** in dichloromethane. The first oxidation process at  $E^0(1)$  is more positive by 60 mV for the V-shaped compound **10a** than for the linear analogue **17a**, whereas the second peak at  $E_{pa}(2)$  remains at the same value for both compounds. This suggests that the incorporation of a second withdrawing group decreases the net electron density on the pyranylidene moiety, making its oxidation at  $E_{pa}(1)$  slightly more difficult than with only one withdrawing group. The same tendency (50-70 mV potential difference) is observed for the di-anchoring compounds **10b**, **10c** and **12c** compared to their mono-anchoring analogues **D1**, **D2** and **D3**, respectively, although measurements have not been carried out in the same conditions (solvent). Interestingly, the  $E^0(1)$  value is almost independent of the R substituting group (R=phenyl, thienyl, *t*-butyl) for V-shaped compounds **10a-c** (see values in CH<sub>2</sub>Cl<sub>2</sub>/THF in Table 2), as for similar linear pyranylidenes (Durand et al., 2017). Scanning towards negative potentials leads to the appearance of broad and irreversible peaks (3) and (4) in the 0.2 V to -0.8 V potential range (*vs.* NHE), corresponding to the reduction of the cyanoacetic anchoring groups, consistently with literature (Gauthier et al., 2014). The appearance of one or two peaks is not clearly understood at this stage. Increasing of the number of thienyl linkers induces a negative shift of the reduction, as clearly emphasized on Fig. 3B with compounds **17a**, **18a** and **19a**, whereas oxidation peaks remain almost unaffected.

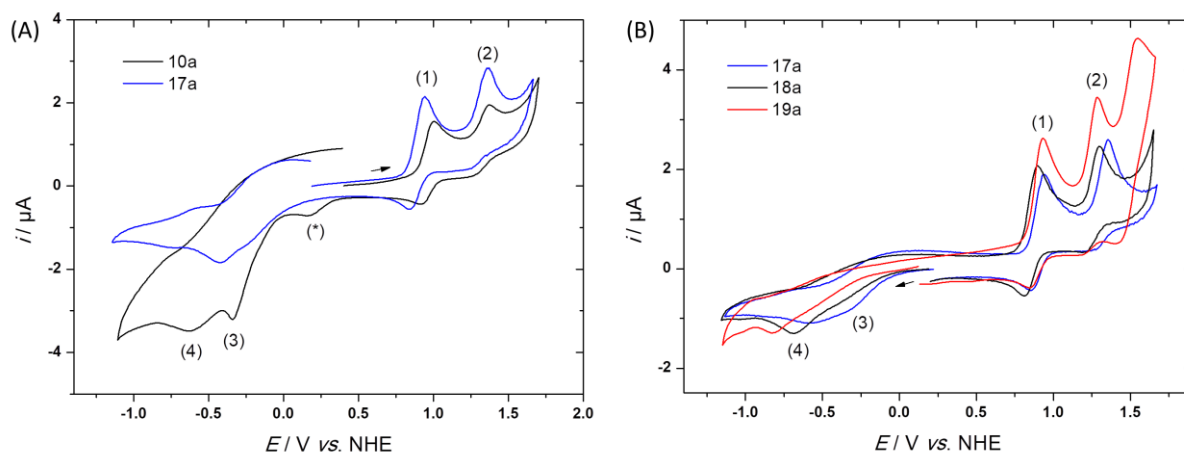


**Fig. 3.** Cyclic voltammetry at a Pt electrode of A) **10a** (black) and **17a** (blue) in positive initial scanning; B) **17a** (blue), **18a** (black) and **19a** (red) in negative initial scanning. Experimental curves were measured in  $\text{CH}_2\text{Cl}_2 / \text{NBu}_4\text{PF}_6$  0.1 M ( $\nu = 0.1 \text{ V s}^{-1}$ ,  $C = 0.5 \text{ mM}$ ). Redox potential values were recalibrated by taking  $E^0(\text{Fc}^+/\text{Fc}) = 0.71 \text{ V vs. NHE}$ . Peak (\*): not observed when scanning in initial negative direction.

**Table 2**

Electrochemical data for **10a-c**, **12c**, **17a**, **18a**, **19a**, **D1**, **D2** and **D3** (0.5 mM) at a Pt working electrode in  $\text{CH}_2\text{Cl}_2/\text{NBu}_4\text{PF}_6$  0.1 M ( $E / \text{V vs. NHE}^a$ ,  $\nu = 0.1 \text{ V s}^{-1}$ ).  $\Delta G_{\text{inj}}$  and  $\Delta G_{\text{reg}}$  values for **10a-c**, **12c**, **17a**, **18a**, **19a**, **D1**, **D2** and **D3**.

| Dye                     | $E^0(1)^a$ | $E_{\text{pa}}(2)^a$ | $E_{\text{pc}}(3)^{a,b}$ | $E_{\text{pc}}(4)^{a,b}$ | $E(\text{S}^*/\text{S}^+)^c$ | $\Delta G_{\text{reg}}^d$ | $\Delta G_{\text{inj}}^d$ |
|-------------------------|------------|----------------------|--------------------------|--------------------------|------------------------------|---------------------------|---------------------------|
| <b>10a</b> <sup>f</sup> | 0.96       | 1.35 <sup>b</sup>    | -0.37                    | -0.81                    | -1.22                        | -0.61                     | -0.72                     |
| <b>10b</b> <sup>g</sup> | 1.02       | 1.28 <sup>b</sup>    | <sup>e</sup>             | -0.75                    | -1.21                        | -0.67                     | -0.71                     |
| <b>10c</b> <sup>g</sup> | 1.03       | 1.28 <sup>b</sup>    | <sup>e</sup>             | -0.83                    | -1.17                        | -0.68                     | -0.67                     |
| <b>12c</b> <sup>h</sup> | 0.97       | <sup>e</sup>         | <sup>e</sup>             | -0.91                    | -1.00                        | -0.62                     | -0.50                     |
| <b>17a</b>              | 0.90       | 1.35 <sup>b</sup>    | -0.29                    | -0.57                    | -1.30                        | -0.55                     | -0.79                     |
| <b>18a</b>              | 0.87       | 1.30 <sup>b</sup>    | <sup>e</sup>             | -0.68                    | -1.42                        | -0.52                     | -0.92                     |
| <b>19a</b>              | 0.89       | 1.29 <sup>b</sup>    | <sup>e</sup>             | -0.81                    | -1.41                        | -0.54                     | -0.91                     |
| <b>D1</b> <sup>i</sup>  | 0.97       | 1.33                 | -0.47                    | -0.83                    | -1.21                        | -0.62                     | -0.71                     |
| <b>D2</b> <sup>i</sup>  | 0.98       | 1.27                 | <sup>e</sup>             | -0.65                    | -1.20                        | -0.63                     | -0.70                     |
| <b>D3</b> <sup>i</sup>  | 0.90       | 1.11                 | -0.55                    | -0.79                    | -0.99                        | -0.55                     | -0.49                     |

<sup>a</sup> Values calibrated vs. NHE from the experimental curves obtained vs.  $\text{Fc}^+/\text{Fc}$ , by taking  $E^0(\text{Fc}^+/\text{Fc}) = 0.47 \text{ V vs. SCE}$  in  $\text{CH}_2\text{Cl}_2/\text{NBu}_4\text{PF}_6$  (measured experimentally) and  $E^0(\text{SCE}) = 0.24 \text{ V vs. NHE}$ .

<sup>b</sup> Irreversible peak

<sup>c</sup>  $E(\text{S}^*/\text{S}^+)$ : Fermi level (in V vs. NHE) of excited molecules, calculated from :

$E(\text{S}^*/\text{S}^+) = E^0(1) - \Delta E_{0-0}(\text{S}/\text{S}^*)$ , where  $\Delta E_{0-0}$  is the stored excitation energy, obtained from  $\lambda_{\text{onset}}$ .

<sup>d</sup>  $\Delta G$  in eV,  $\Delta G_{\text{reg}} = E^0(\text{I}/\text{I}_3^-) - E^0(1)$  with  $E^0(\text{I}/\text{I}_3^-) = 0.35 \text{ V vs. NHE}$ ;  $\Delta G_{\text{inj}} = E(\text{S}^*/\text{S}^+) - E_{\text{CB}}(\text{TiO}_2)$  with  $E_{\text{CB}}(\text{TiO}_2) = -0.5 \text{ V vs. NHE}$ .

<sup>e</sup> Peak not detected.

<sup>f</sup> For comparison with compounds **10b** and **10c**, the values found in  $\text{CH}_2\text{Cl}_2/\text{THF}$  (50:50 v:v) /  $\text{NBu}_4\text{PF}_6$  0.1 M are as following:  $E^0(1) = 0.98 \text{ V vs. NHE}$ ;  $E_{\text{pa}}(2) = 1.34 \text{ V vs. NHE}$ ;  $E_{\text{pc}}(4) = -0.77 \text{ V vs. NHE}$ ;  $E(\text{S}^*/\text{S}^+) = -1.28 \text{ V vs. NHE}$ ;  $\Delta G_{\text{reg}} = -0.63 \text{ V vs. NHE}$ ;  $\Delta G_{\text{inj}} = -0.78 \text{ V vs. NHE}$ .

<sup>g</sup> Compound poorly soluble in CH<sub>2</sub>Cl<sub>2</sub>. Experiment performed in CH<sub>2</sub>Cl<sub>2</sub> / THF (50:50 v:v) / NBu<sub>4</sub>PF<sub>6</sub> 0.1 M.

<sup>h</sup> Compound poorly soluble in CH<sub>2</sub>Cl<sub>2</sub> and CH<sub>2</sub>Cl<sub>2</sub> / THF (50:50 v:v). Experiment performed in THF / NBu<sub>4</sub>PF<sub>6</sub> 0.1 M.

<sup>i</sup> (Gauthier et al., 2019).

## 2.4. Quantum chemical calculations

To describe the electronic transitions, and especially to quantify the ICT strength of all molecular structures presented in this paper, we performed (Time-Dependent) Density Functional Theory Calculations using a range-separated hybrid (see the SI for computational details). The optimal ground-state geometries of all compounds did not reveal any unexpected aspect. For instance, in **17a**, the cyanoacrylic, thienyl, and ethynyl-phenyl moieties are almost perfectly coplanar (dihedral < 1°), whereas the pyranilidene moiety and the two vicinal six-member rings are arranged in a propeller-shape with respect to each other with dihedral angle in the 42-52° range. The frontier orbitals HOMO and LUMO are displayed in Fig. 4 for **10a** and in Fig. S43 (SI) for the other dyes. As can be seen, the HOMO is centered on the electron-donor pyranilidene moiety, while the LUMO is split between the two accepting branches of the dye, with strong contributions on both the cyanoacrylic and the thienyl moieties. This clearly indicates that the synthesized dyes have the appropriate HOMO and LUMO localizations for DSSC applications as the directionality of the change of electronic density upon absorption of light is favorable for electron injection into the semiconductor conduction band.

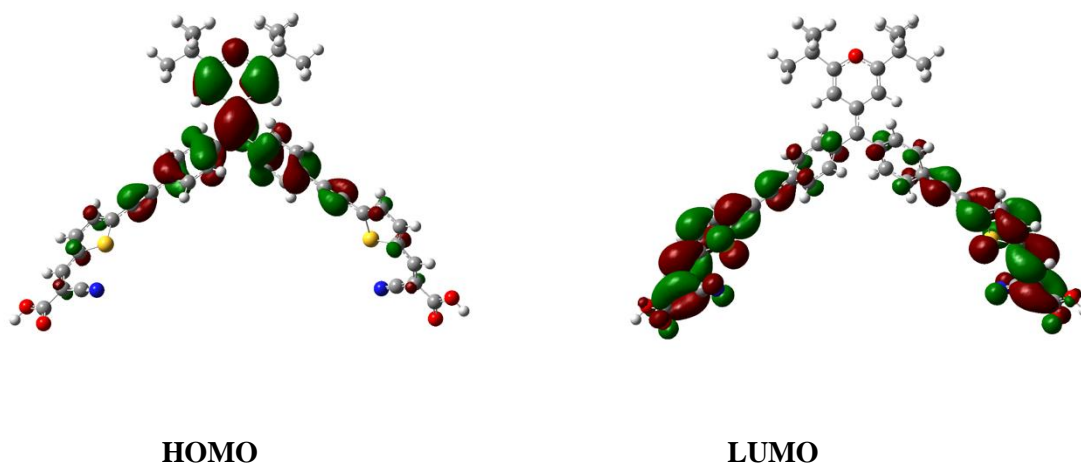


**Fig. 4.** Contour plots of the CAM-B3LYP HOMO and LUMO orbitals of dye **10a**.

TD-DFT was used to obtain the vertical transition energies as well as the ICT parameters following Le Bahers'  $d_{CT}$  metric (Jacquemin et al., 2012; Le Bahers et al., 2011). The results are shown in Table 3. First, the systems with two anchoring groups display two nearly degenerated states, corresponding to transitions from the HOMO to the LUMO and LUMO+1, the latter two combining orbitals localized on the two anchoring branches (see the SI). While it is important to mention that the computed TD-DFT transition energies in the vertical approximation cannot be strictly compared to experimental wavelength of maximal absorption, we can still notice that the computed transition wavelengths are in good qualitative agreement with experimental trends with *i*) almost no spectral change in **10a**, **10b**, and **10c**, which is consistent with the lack of contribution of the substituting groups (*t*-butyl, phenyl and thienyl) on the density difference plots (Fig. 5); *ii*) a significant redshift when going from **10c** to **12c**; *iii*) red and hyperchromic shifts in the **17a**, **18a** and **19a** series. Additionally, the energies of the frontier MOs are not strongly affected by substitution (see the SI), which confirms the electrochemical study described above. As can be seen in Table 3, all the lowest transitions involve strong ICT with a charge transfer of ca. 0.6-0.8 electron over several Å. The values given in Table 3 are large compared to those reported in the literature obtained with a very similar approach (Ciofini et al., 2012). When going from **17a**,

to **18a** and then **19a**, the bands are redshifted, but this is not accompanied with an increase of the ICT character. On the contrary, the ICT character decreases, which is understandable from the density difference plots shown on Fig. 5. While **17a** displays a net ICT from the donor group to the accepting moiety, in **19a**, the donor group becomes a more passive element, and the ICT starts from the oligothiophene bridge to the cyanoacrylic moiety. This confirms that longer linkers do not necessarily provide an improved ICT character (Jacquemin et al., 2012). We also noted that the ICT properties of **17a** were similar to these of the previously described **D1** and **D2** (Gauthier et al., 2019). Our theoretical study shows that all di-anchoring dyes display a strong ICT from the electron donor pyranilidene core to the accepting groups on the two branches (see also the SI for density difference plots for the second state), indicating that these dyes could be attractive candidates for DSSC applications.

**Table 3**

Theoretical vertical excitation wavelength [PCM(THF)-CAM-B3LYP/6-311+G(2d,p)] in nm, oscillator strength (between brackets) and Le Bahers' ICT parameters of all dyes:  $d_{CT}$  and  $q_{CT}$  are given in Å and in e, respectively.

| Dye                   | $\lambda^{vert}/nm$ | $d_{CT}/\text{Å}$ | $q_{CT}/e$ |
|-----------------------|---------------------|-------------------|------------|
| <b>10a</b>            | 472 (1.41)          | 3.97              | 0.82       |
|                       | 462 (1.68)          | 3.78              | 0.71       |
| <b>10b</b>            | 474 (1.96)          | 3.51              | 0.63       |
|                       | 467 (1.44)          | 4.21              | 0.80       |
| <b>10c</b>            | 482 (1.98)          | 3.41              | 0.61       |
|                       | 468 (1.44)          | 4.32              | 0.78       |
| <b>12c</b>            | 538 (1.21)          | 2.08              | 0.56       |
|                       | 522 (2.05)          | 3.09              | 0.79       |
| <b>17a</b>            | 478 (1.48)          | 5.62              | 0.82       |
| <b>18a</b>            | 484 (2.14)          | 5.54              | 0.66       |
| <b>19a</b>            | 495 (2.32)          | 4.78              | 0.60       |
| <b>D1<sup>a</sup></b> | 480 (1.6)           | 5.50              | 0.75       |
| <b>D2<sup>a</sup></b> | 485 (1.6)           | 5.44              | 0.73       |
| <b>D3<sup>a</sup></b> | 554 (1.4)           | 4.55              | 0.68       |

<sup>a</sup>(Gauthier et al., 2019).

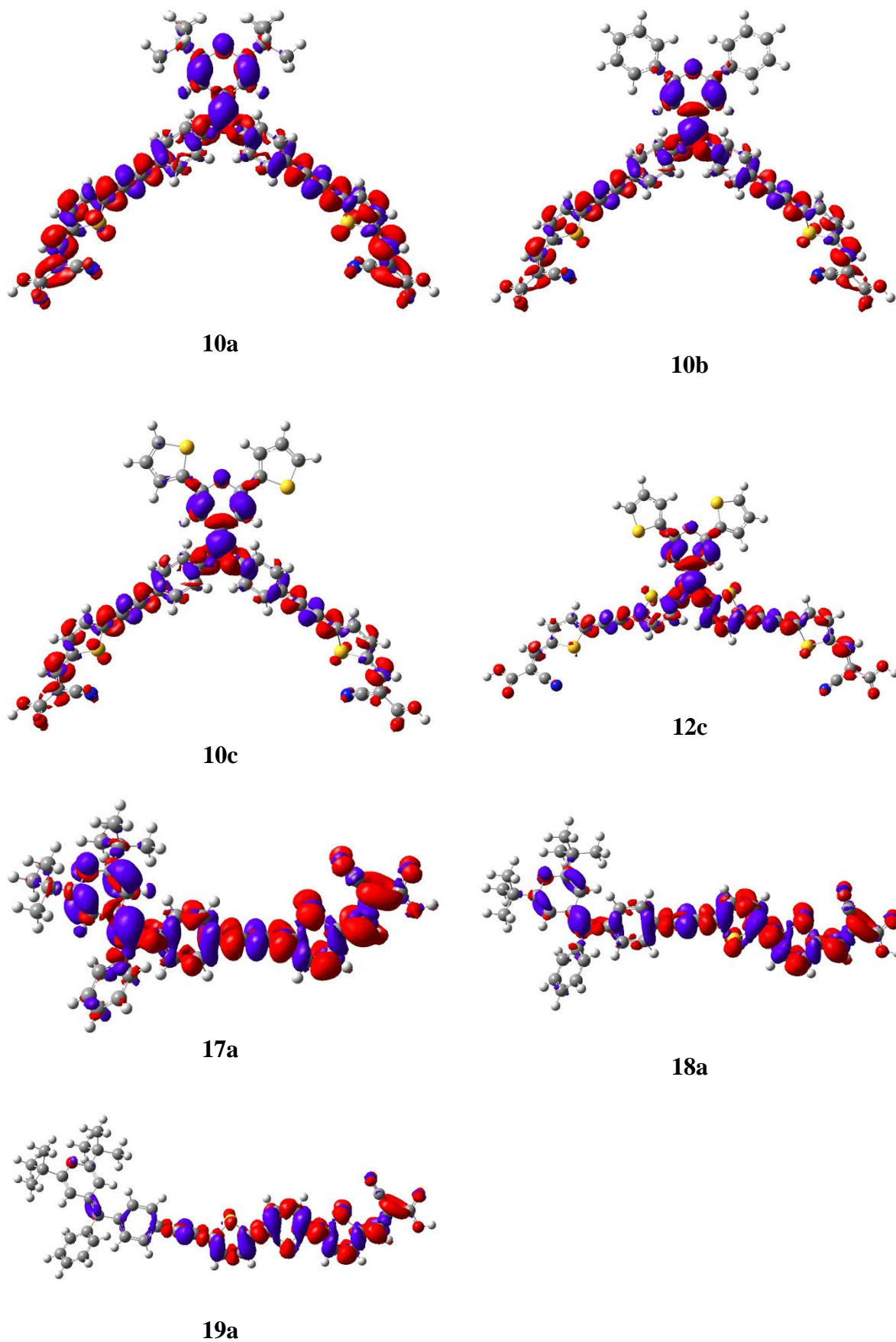


**Fig. 5.** EDD plots calculated for the lowest transition of all dyes. The blue (red) lobes represent regions of density increase (decrease) upon excitation. See also the SI. Contour threshold: 0.0008 au.

## 2.5. Photovoltaic measurements

All photosensitizers were used to dye TiO<sub>2</sub> mesoporous electrodes (12 μm thick) using the conditions optimized in our previous work (Gauthier et al., 2019). Briefly, the TiO<sub>2</sub> photo-electrodes were immersed in a mixture of tert-butanol and acetonitrile which was used to dissolve the organic molecules (0.25 mM) in presence of 1 mM chenodeoxycholic acid whose role is to limit the aggregation of the dyes on the semi-conductor. Aggregation is known to promote the premature deactivation of the excited state of the chemisorbed dye and dramatically affects the performances of the solar devices (Zhang and Cole, 2017). After one night, the obtained photo-electrodes were rinsed, quickly assembled with a platinum counter-electrode and impregnated with a triiodide/iodide electrolyte. The detailed fabrication of the devices is given in the Supporting Information and the current/voltage characteristic of the cells are gathered in Figure S45. The Incident Photon-to-Electron Conversion Efficiency (IPCE) for all dyes are given in Fig. 6, and indicate that the pyranilidene dyes exhibit good sensitizing properties with light absorption capacity extending as far as about 650 nm.

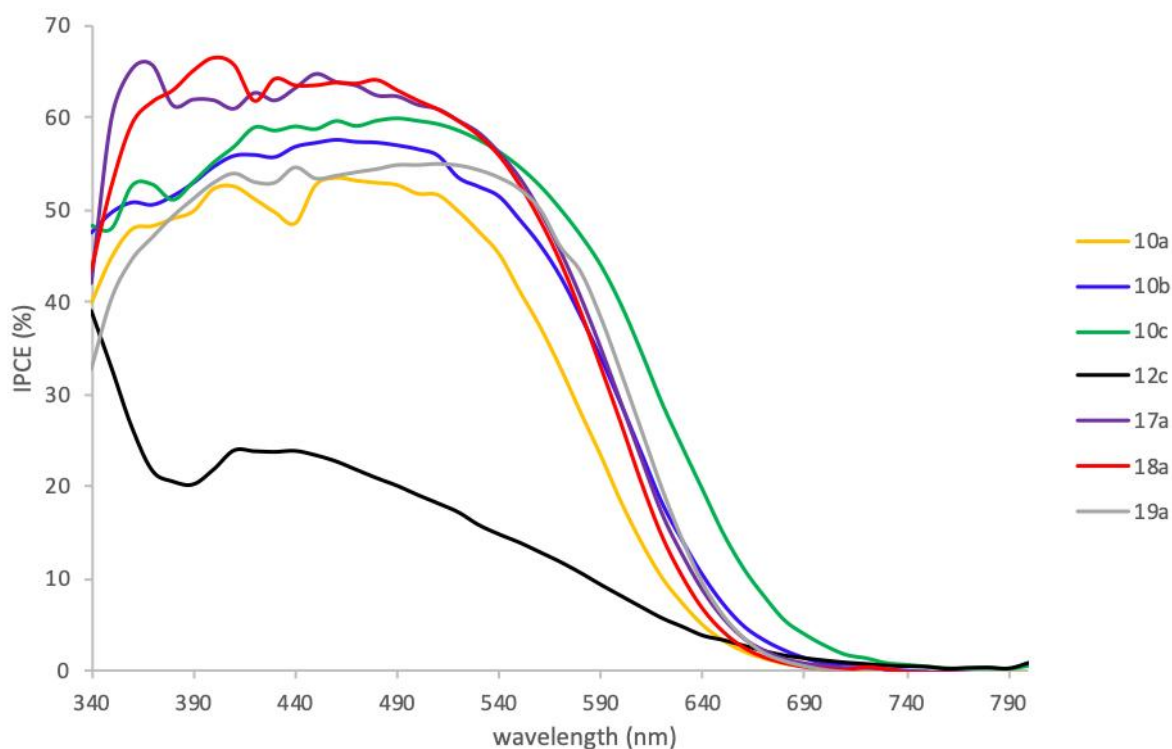


**Fig. 6.** IPCE of the DSSC using dyes **10a-c**, **12c**, **17a**, **18a**, and **19a** as photosensitizers.

**Table 4**

Metrics of the solar cells fabricated illuminated with a calibrated sunlight AM1.5 (100 mW/cm<sup>2</sup>). Electron lifetime recorded by IMVS at 150 W/m<sup>2</sup> irradiance.

| Dye                   | Jsc (mA/cm <sup>2</sup> ) | Voc (mV) | FF (%)  | PCE (%)      | Dye loading (nmol/cm <sup>2</sup> ) | Electron lifetime (ms) |
|-----------------------|---------------------------|----------|---------|--------------|-------------------------------------|------------------------|
| <b>10a</b>            | 8.26 (±0.40)              | 565 (±4) | 72 (±1) | 3.35 (±0.16) | 79.2                                | 40.1                   |
| <b>10b</b>            | 8.52 (±0.35)              | 532 (±1) | 72 (±1) | 3.25 (±0.16) | 95.8                                | 31.8                   |
| <b>10c</b>            | 9.74 (±0.28)              | 538 (±5) | 68 (±2) | 3.57 (±0.18) | 110.4                               | 25.3                   |
| <b>12c</b>            | 4.75 (±0.60)              | 492 (±4) | 70 (±1) | 1.64 (±0.22) | 67.5                                | 14.2                   |
| <b>17a</b>            | 11.43 (±0.10)             | 652 (±4) | 70 (±1) | 5.23 (±0.11) | 110.3                               | 52.6                   |
| <b>18a</b>            | 9.84 (±0.80)              | 612 (±1) | 72 (±1) | 4.32 (±0.32) | 138.0                               | 60.8                   |
| <b>19a</b>            | 9.73 (±0.06)              | 574 (±1) | 70 (±1) | 3.90 (±0.09) | 137.4                               | 46.9                   |
| <b>D1<sup>a</sup></b> | 13.1 (±0.1)               | 603 (±1) | 70 (±1) | 5.52 (±0.01) | 174                                 | 43.67                  |
| <b>D2<sup>a</sup></b> | 10.8 (±0.1)               | 588 (±4) | 70 (±1) | 4.44 (±0.03) | 173                                 | 24.19                  |
| <b>D3<sup>a</sup></b> | 6.7 (±0.1)                | 505 (±1) | 68 (±1) | 2.31 (±0.05) | 161                                 | 13.70                  |

<sup>a</sup> (Gauthier et al., 2019).

The devices were then tested under AM 1.5 calibrated irradiation. Their performances are gathered in Table 4. At first glance, it appears clearly that the di-anchoring dyes are less performant than their analogues mono-anchoring dyes because of lesser Jsc and Voc. This is particularly obvious when comparing **10a** with **17a**, whose structures only differ by the number of anchoring sites (2 vs. 1 respectively). However, this observation can be extended to the sub-series **10a**, **10b**, **10c** and **12c** vs. sub-series **17a**, **18a** and **19a** where substituents in positions 2 and 6 of the pyranilidene core are different, but known to only marginally affect

the photovoltaic parameters (Gauthier et al., 2019). Within the di-anchoring dye series,  $J_{sc}$  increases in the following order: **12c**<<**10a**<**10b**<<**10c**. The dye **12c** exhibits the lowest injection driving force (Table 4), combined with the lowest dye loading (Table 4) and the lowest  $d_{CT}$  (Table 3) in the series, thus justifying its ranking as the least performant dye. **10a**, **10b** and **10c** display comparable injection driving forces. Their charge transfers, quantitatively estimated by  $d_{CT}$  and  $q_{CT}$  (Table 3) are also similar and, therefore, the observed increase in  $J_{sc}$  more likely stems from the increasing dyes loading which follows a similar ranking: **12c**<<**10a**<**10b**<<**10c**. Moreover, the absorption spectrum of **10c** is the most intense between 400-550 nm implying a higher light harvesting efficiency.

The open circuit potential  $V_{oc}$  decreases in the following order: **10a**>**10b**≈**10c**>**12c**. The  $V_{oc}$  is the difference of the Nernst potential of the counter-electrode and the Fermi level energy of the dyed  $TiO_2$  photo-electrode. The latter is strongly affected by electrostatic and dipolar interactions between the  $TiO_2$  surface and the dye (thermodynamic parameters) as well as by the charge recombination processes occurring at the dye/ $TiO_2$  interface, *e.g.* between triiodide or oxidized dye (after electron injection) and the electrons diffusing in the semi-conductor conduction band (kinetic parameters). Since the same conditions were used to prepare the  $TiO_2$  photo-electrodes (electrolyte, substrate...) and the ICT characters of di-anchoring dyes **10a**, **10b** and **10c** are comparable, thermodynamic effects are unlikely to account for this observation. Dye **10a** is, however, considerably bulkier than dyes **10b**, **10c** and **12c** due to the bulky *t*-butyl groups: this implies that the triiodide ions will experience more difficulties to penetrate the dye monolayer, and consequently to reach the  $TiO_2$  surface. Thus, the surface is more passivated, hence limiting interfacial charge recombination and leading to the highest  $V_{oc}$  in the di-anchoring dyes series. The average electron lifetime in  $TiO_2$  was measured by Intensity- Modulated photovoltage Spectroscopy (IMVS) experiments. The electron lifetimes measured by IMVS are ranked in the following order: **10a**>>**10b**>**10c**>>**12c** which fully

supports the results described above for these dyes (Table 4 and Figure S46, SI), meaning that the TiO<sub>2</sub> surface shielding by the dye is maximum with *t*-butyl groups (dye **10a**) and minimal with thienyl substituents (**10c** and **12c**).

The DSSC features of the mono-anchoring dyes **17a**, **D1**, **D2** and **D3** display significantly better performances than their di-anchoring dye counterparts because of higher J<sub>sc</sub> and higher Voc. This is due to several factors. First, the mono-anchoring dyes are substantially less bulky than the di-anchoring ones, and consequently display a much higher dye surface loading capacity, thus leading to a more favorable light harvesting efficiency and consequently higher J<sub>sc</sub>. In addition, injection driving forces and calculated d<sub>CT</sub> and q<sub>CT</sub> (Table 3) are more favorable for mono-anchoring dyes than for di-anchoring dyes, thus favoring a high J<sub>sc</sub>. Finally, mono-anchoring dyes **18a** and **19a** exhibit a more intense absorption band in the 450-550 nm region, (therefore a higher light harvesting efficiency) than di-anchoring systems (Fig. 2), which favors the creation of a large photocurrent density since the photon flux of the solar spectrum is very intense in this region.

The better performances of the mono-anchoring dyes also originate from larger Voc. This can be assigned to the higher quality of the dye monolayer formed by the mono-anchoring dyes. As mentioned above, the higher dye loading capacity of the mono-anchoring dyes and the presence of *t*-butyl groups lead to a dense organic passivating layer, which prevent interfacial charge recombination with triiodide. IMVS data confirm this assertion since the electron lifetime is shorter for di-anchoring dyes than for all mono-anchoring ones. Interestingly, the Voc decrease within the mono-anchoring series in the following order: **17a**>**18a**>**19a**. Namely, the output potential diminishes when the size of the oligothieryl spacers increases (from one to three thienyl units) and follows the same trend as the ICT character (Table 3) which can also induce a higher upward band bending of the conduction band of TiO<sub>2</sub> (Rühle et al., 2005; Zhang and Yates, 2012). A similar observation was made in previous works

(Gauthier et al., 2019) where we also attributed the output potential decrease to a plausible bending of the dye backbone due to oligothieryl structure, to an increased aggregation or to a closer distance with the TiO<sub>2</sub> surface.

### 3. Conclusions

In this work, seven new push-pull sensitizers were synthesized and investigated for their photovoltaic performances in DSSC. The originality of this work stems from the synthesis of V-shaped di-anchoring D-( $\pi$ -A)<sub>2</sub> dyes containing the pyranilidene group as electron donor. Such structures have been much less investigated than similar molecular systems based on trisarylamine moieties for DSSCs applications.

The major goal of this work was to investigate the impact of: i) the substituents on the pyranilidene group and ii) the number of anchoring groups of the dyes on the photovoltaic performances of the sensitizers. First, we found that the *t*-butyl substituents on the pyranilidene group resulted in better photovoltaic performances than the phenyl or thienyl ones, as the *t*-butyl moiety impose specific dye loading and conformation on the TiO<sub>2</sub> surface, which prevents interfacial charge recombination. Interestingly, the substituents in 2,6 positions on the pyranilidene group barely affect the electronic properties of the dyes, but have a significant impact on the structure and the organization of the dye on the TiO<sub>2</sub> surface.

The second major finding of this study is that the binding of these types of dyes to the TiO<sub>2</sub> surface through two anchoring sites does not seem to enhance photovoltaic performances, and the di-anchoring dyes were not found to exhibit systematically superior photovoltaic properties compared to their mono-anchoring counterparts. The higher photovoltaic

performances displayed by the mono-anchoring dyes of this series stem from their lower molecular footprint which allows for a higher dye loading resulting in a better surface shielding from the electrolyte. Moreover, their higher ICT character increases the upward band bending. This investigation has provided valuable pieces of information for the future development of better performing organic push-pull dyes based on pyranilidene as electron-donor group.

### **Acknowledgments**

We thank the *Région des Pays de la Loire*, for financial support via LUMOMAT program.

This work used the computational resources of the CCIPL installed in Nantes.

### **Supplementary material**

Supplementary data to this article (Synthesis and characterization details, Theoretical Calculations and Photovoltaic Measurements) can be found online at ...

### **References**

- Abbotto, A., Manfredi, N., Marinzi, C., De Angelis, F., Mosconi, E., Yum, J.-H., Xianxi, Z., Nazeeruddin, M.K., Grätzel, M., 2009. Di-branched di-anchoring organic dyes for dye-sensitized solar cells. *Energy Environ. Sci.* 2, 1094.
- Alagumalai, A., M. K., M.F., Vellimalai, P., Sil, M.C., Nithyanandhan, J., 2016. Effect of Out-of-Plane Alkyl Group's Position in Dye-Sensitized Solar Cell Efficiency: A Structure–Property Relationship Utilizing Indoline-Based Unsymmetrical Squaraine Dyes. *ACS Appl. Mater. Interfaces* 8, 35353–35367.
- Ambrosio, F., Martsinovich, N., Troisi, A., 2012. What Is the Best Anchoring Group for a Dye in a Dye-Sensitized Solar Cell? *J. Phys. Chem. Lett.* 3, 1531–1535.
- Andrés-Castán, J.M., Andreu, R., Villacampa, B., Orduna, J., Franco, S., 2019. 4H-pyranilidene organic dyes for dye-sensitized solar cells: Twisted structures towards enhanced power conversion efficiencies. *Solar Energy* 193, 74–84.

- Andreu, R., Carrasquer, L., Franco, S., Garín, J., Orduna, J., Martínez de Baroja, N., Alicante, R., Villacampa, B., Allain, M., 2009. 4 *H*-Pyran-4-ylidenes: Strong Proaromatic Donors for Organic Nonlinear Optical Chromophores. *J. Org. Chem.* 74, 6647–6657.
- Bandara, T.M.W.J., Dissanayake, M.A.K.L., Albinsson, I., Mellander, B.-E., 2010. Dye-sensitized, nano-porous TiO<sub>2</sub> solar cell with poly(acrylonitrile): MgI<sub>2</sub> plasticized electrolyte. *Journal of Power Sources* 195, 3730–3734.
- Berhe Desta, M., Chaurasia, S., Lin, J.T., 2017. Reversed Y-shape di-anchoring sensitizers for dye sensitized solar cells based on benzimidazole core. *Dyes and Pigments* 140, 441–451.
- Bessho, T., Zakeeruddin, S.M., Yeh, C.-Y., Diau, E.W.-G., Grätzel, M., 2010. Highly Efficient Mesoscopic Dye-Sensitized Solar Cells Based on Donor-Acceptor-Substituted Porphyrins. *Angewandte Chemie International Edition* 49, 6646–6649.
- Bolag, A., Nishida, J., Hara, K., Yamashita, Y., 2012. Enhanced performance of dye-sensitized solar cells with novel 2,6-diphenyl-4H-pyranylidene dyes. *Organic Electronics* 13, 425–431.
- Brunetti, F.G., López, J.L., Atienza, C., Martín, N., 2012.  $\pi$ -Extended TTF: a versatile molecule for organic electronics. *J. Mater. Chem.* 22, 4188.
- Cai, N., Li, R., Wang, Y., Zhang, M., Wang, P., 2013. Organic dye-sensitized solar cells with a cobalt redox couple: influences of  $\pi$ -linker rigidification and dye-bath solvent selection. *Energy Environ. Sci.* 6, 139–147.
- Choi, H., Baik, C., Kang, S.O., Ko, J., Kang, M.-S., Nazeeruddin, Md.K., Grätzel, M., 2008. Highly Efficient and Thermally Stable Organic Sensitizers for Solvent-Free Dye-Sensitized Solar Cells. *Angew. Chem. Int. Ed.* 47, 327–330.
- Ciofini, I., Le Bahers, T., Adamo, C., Odobel, F., Jacquemin, D., 2012. Through-Space Charge Transfer in Rod-Like Molecules: Lessons from Theory. *J. Phys. Chem. C* 116, 11946–11955.
- Durand, R.J., Gauthier, S., Achelle, S., Groizard, T., Kahlal, S., Saillard, J.-Y., Barsella, A., Le Poul, N., Le Guen, F.R., 2018. Push–pull D– $\pi$ –Ru– $\pi$ –A chromophores: synthesis and electrochemical, photophysical and second-order nonlinear optical properties. *Dalton Trans.* 47, 3965–3975.
- Durand, R.J., Gauthier, S., Achelle, S., Kahlal, S., Saillard, J.-Y., Barsella, A., Wojcik, L., Le Poul, N., Robin-Le Guen, F., 2017. Incorporation of a platinum center in the  $\pi$ -conjugated core of push–pull chromophores for nonlinear optics (NLO). *Dalton Trans.* 46, 3059–3069.
- Ferreira, E., Le Poul, P., Cabon, N., Caro, B., Robin-Le Guen, F., Pellegrin, Y., Planchat, A., Odobel, F., 2017. New D– $\pi$ –A-conjugated organic sensitizers based on  $\alpha$ -pyranylidene donors for dye-sensitized solar cells. *Tetrahedron Letters* 58, 995–999.
- Fischer, M.K.R., Wenger, S., Wang, M., Mishra, A., Zakeeruddin, S.M., Grätzel, M., Bäuerle, P., 2010. D– $\pi$ –A Sensitizers for Dye-Sensitized Solar Cells: Linear vs Branched Oligothiophenes. *Chem. Mater.* 22, 1836–1845.
- Gauthier, S., Caro, B., Robin-Le Guen, F., Bhuvanesh, N., Gladysz, J.A., Wojcik, L., Le Poul, N., Planchat, A., Pellegrin, Y., Blart, E., Jacquemin, D., Odobel, F., 2014. Synthesis, photovoltaic performances and TD-DFT modeling of push–pull diacetylide platinum complexes in TiO<sub>2</sub> based dye-sensitized solar cells. *Dalton Trans.* 43, 11233–11242.
- Gauthier, S., Porter, A., Achelle, S., Roisnel, T., Dorcet, V., Barsella, A., Le Poul, N., Guevara Level, P., Jacquemin, D., Robin-Le Guen, F., 2018. Mono- and Diplatinum Polyynediyl Complexes as Potential Push–Pull Chromophores: Synthesis, Characterization, TD-DFT Modeling, and Photophysical and NLO Properties. *Organometallics* 37, 2232–2244.

- Gauthier, S., Robin-Le Guen, F., Wojcik, L., Le Poul, N., Planchat, A., Pellegrin, Y., Level, P.G., Szuwarski, N., Boujtita, M., Jacquemin, D., Odobel, F., 2019. Synthesis and properties of novel pyranilidene-based organic sensitizers for dye-sensitized solar cells. *Dyes and Pigments* 171, 107747.
- Gauthier, S., Vologdin, N., Achelle, S., Barsella, A., Caro, B., Robin-le Guen, F., 2013. Methylenepyran based dipolar and quadrupolar dyes: synthesis, electrochemical and photochemical properties. *Tetrahedron* 69, 8392–8399.
- Grätzel, M., 2009. Recent Advances in Sensitized Mesoscopic Solar Cells. *Acc. Chem. Res.* 42, 1788–1798.
- Grisorio, R., De Marco, L., Allegretta, G., Giannuzzi, R., Suranna, G.P., Manca, M., Mastroilli, P., Gigli, G., 2013. Anchoring stability and photovoltaic properties of new D( $\pi$ -A)<sub>2</sub> dyes for dye-sensitized solar cell applications. *Dyes and Pigments* 98, 221–231.
- Gupta, K.S.V., Suresh, T., Singh, S.P., Islam, A., Han, L., Chandrasekharam, M., 2014. Carbazole based A- $\pi$ -D- $\pi$ -A dyes with double electron acceptor for dye-sensitized solar cell. *Organic Electronics* 15, 266–275.
- Hagfeldt, A., Boschloo, G., Sun, L., Kloo, L., Pettersson, H., 2010. Dye-Sensitized Solar Cells. *Chem. Rev.* 110, 6595–6663.
- Higashino, T., Imahori, H., 2015. Porphyrins as excellent dyes for dye-sensitized solar cells: recent developments and insights. *Dalton Trans.* 44, 448–463.
- Horiuchi, T., Miura, H., Uchida, S., 2003. Highly-efficient metal-free organic dyes for dye-sensitized solar cells. *Chem. Commun.* 3036.
- Hsu, H.-Y., Wang, C.-Y., Fathi, A., Shiu, J.-W., Chung, C.-C., Shen, P.-S., Guo, T.-F., Chen, P., Lee, Y.-P., Diau, E.W.-G., 2014. Femtosecond Excitonic Relaxation Dynamics of Perovskite on Mesoporous Films of Al<sub>2</sub>O<sub>3</sub> and NiO Nanoparticles. *Angew. Chem. Int. Ed.* 53, 9339–9342.
- Imahori, H., Umeyama, T., Ito, S., 2009. Large  $\pi$ -Aromatic Molecules as Potential Sensitizers for Highly Efficient Dye-Sensitized Solar Cells. *Acc. Chem. Res.* 42, 1809–1818.
- Jacquemin, D., Bahers, T.L., Adamo, C., Ciofini, I., 2012. What is the “best” atomic charge model to describe through-space charge-transfer excitations? *Phys. Chem. Chem. Phys.* 14, 5383.
- Ji, J.-M., Zhou, H., Kim, H.K., 2018. Rational design criteria for D- $\pi$ -A structured organic and porphyrin sensitizers for highly efficient dye-sensitized solar cells. *J. Mater. Chem. A* 6, 14518–14545.
- Jia, H., Shen, K., Ju, X., Zhang, M., Zheng, H., 2016. Enhanced performance of dye-sensitized solar cells with Y-shaped organic dyes containing di-anchoring groups. *New J. Chem.* 40, 2799–2805.
- Le Bahers, T., Adamo, C., Ciofini, I., 2011. A Qualitative Index of Spatial Extent in Charge-Transfer Excitations. *J. Chem. Theory Comput.* 7, 2498–2506.
- Lewis, N.S., Nocera, D.G., 2006. Powering the planet: Chemical challenges in solar energy utilization. *Proceedings of the National Academy of Sciences* 103, 15729–15735.
- Li, Yuanhao, Song, P., Yang, Y., Ma, F., Li, Yuanzuo, 2017. Double-anchoring organic dyes for dye-sensitized solar cells: the opto-electronic property and performance. *New J. Chem.* 41, 12808–12829.
- Liang, M., Chen, J., 2013. Arylamine organic dyes for dye-sensitized solar cells. *Chem. Soc. Rev.* 42, 3453.
- Luo, J., Wan, Z., Jia, C., Wang, Y., Wu, X., Yao, X., 2016. Co-sensitization of Dithiafulvenyl-Phenothiazine Based Organic Dyes with N719 for Efficient Dye-Sensitized Solar Cells. *Electrochimica Acta* 211, 364–374.

- Mao, J., He, N., Ning, Z., Zhang, Q., Guo, F., Chen, L., Wu, W., Hua, J., Tian, H., 2012. Stable Dyes Containing Double Acceptors without COOH as Anchors for Highly Efficient Dye-Sensitized Solar Cells. *Angew. Chem. Int. Ed.* 51, 9873–9876.
- Marco, A.B., Andreu, R., Franco, S., Garín, J., Orduna, J., Villacampa, B., Diosdado, B.E., López Navarrete, J.T., Casado, J., 2013. Push–pull systems bearing a quinoid/aromatic thieno[3,2-b]thiophene moiety: synthesis, ground state polarization and second-order nonlinear properties. *Org. Biomol. Chem.* 11, 6338.
- Marco, A.B., Burrezo, P.M., Mosteo, L., Franco, S., Garín, J., Orduna, J., Diosdado, B.E., Villacampa, B., López Navarrete, J.T., Casado, J., Andreu, R., 2015. Polarization, second-order nonlinear optical properties and electrochromism in 4H-pyranylidene chromophores with a quinoid/aromatic thiophene ring bridge. *RSC Adv.* 5, 231–242.
- Marco, A.B., Martínez de Baroja, N., Andrés-Castán, J.M., Franco, S., Andreu, R., Villacampa, B., Orduna, J., Garín, J., 2019. Pyranilydene/thienothiophene-based organic sensitizers for dye-sensitized solar cells. *Dyes and Pigments* 161, 205–213.
- Marszalek, M., Nagane, S., Ichake, A., Humphry-Baker, R., Paul, V., Zakeeruddin, S.M., Grätzel, M., 2013. Structural variations of D– $\pi$ –A dyes influence on the photovoltaic performance of dye-sensitized solar cells. *RSC Adv.* 3, 7921.
- Mishra, A., Fischer, M.K.R., Bäuerle, P., 2009. Metal-Free Organic Dyes for Dye-Sensitized Solar Cells: From Structure: Property Relationships to Design Rules. *Angew. Chem. Int. Ed.* 48, 2474–2499.
- Ooyama, Y., Harima, Y., 2012. Photophysical and Electrochemical Properties, and Molecular Structures of Organic Dyes for Dye-Sensitized Solar Cells. *ChemPhysChem* 13, 4032–4080.
- O'Regan, B., Grätzel, M., 1991. A low-cost, high-efficiency solar cell based on dye-sensitized colloidal TiO<sub>2</sub> films. *Nature* 353, 737–740.
- Qu, S., Hua, J., Tian, H., 2012. New D– $\pi$ –A dyes for efficient dye-sensitized solar cells. *Sci. China Chem.* 55, 677–697.
- Rühle, S., Greenshtein, M., Chen, S.-G., Merson, A., Pizem, H., Sukenik, C.S., Cahen, D., Zaban, A., 2005. Molecular Adjustment of the Electronic Properties of Nanoporous Electrodes in Dye-Sensitized Solar Cells. *J. Phys. Chem. B* 109, 18907–18913.
- Sathiyam, G., Sivakumar, E.K.T., Ganesamoorthy, R., Thangamuthu, R., Sakthivel, P., 2016. Review of carbazole based conjugated molecules for highly efficient organic solar cell application. *Tetrahedron Letters* 57, 243–252.
- Soni, S.S., Fadadu, K.B., Vaghasiya, J.V., Solanki, B.G., Sonigara, K.K., Singh, A., Das, D., Iyer, P.K., 2015. Improved molecular architecture of D– $\pi$ –A carbazole dyes: 9% PCE with a cobalt redox shuttle in dye sensitized solar cells. *J. Mater. Chem. A* 3, 21664–21671.
- Srinivas, K., Yesudas, K., Bhanuprakash, K., Rao, V.J., Giribabu, L., 2009. A Combined Experimental and Computational Investigation of Anthracene Based Sensitizers for DSSC: Comparison of Cyanoacrylic and Malonic Acid Electron Withdrawing Groups Binding onto the TiO<sub>2</sub> Anatase (101) Surface. *J. Phys. Chem. C* 113, 20117–20126.
- Wan, Z., Jia, C., Duan, Y., Chen, X., Li, Z., Lin, Y., 2014. Novel organic sensitizers containing dithiafulvenyl units as additional donors for efficient dye-sensitized solar cells. *RSC Adv.* 4, 34896.
- Wang, J., Liu, K., Ma, L., Zhan, X., 2016. Triarylamine: Versatile Platform for Organic, Dye-Sensitized, and Perovskite Solar Cells. *Chem. Rev.* 116, 14675–14725.
- Wang, P., Klein, C., Humphry-Baker, R., Zakeeruddin, S.M., Grätzel, M., 2005. A High Molar Extinction Coefficient Sensitizer for Stable Dye-Sensitized Solar Cells. *J. Am. Chem. Soc.* 127, 808–809.

- Wenger, S., Bouit, P.-A., Chen, Q., Teuscher, J., Censo, D.D., Humphry-Baker, R., Moser, J.-E., Delgado, J.L., Martín, N., Zakeeruddin, S.M., Grätzel, M., 2010. Efficient Electron Transfer and Sensitizer Regeneration in Stable  $\pi$ -Extended Tetrathiafulvalene-Sensitized Solar Cells. *J. Am. Chem. Soc.* 132, 5164–5169.
- Wiberg, J., Marinado, T., Hagberg, D.P., Sun, L., Hagfeldt, A., Albinsson, B., 2009. Effect of Anchoring Group on Electron Injection and Recombination Dynamics in Organic Dye-Sensitized Solar Cells. *J. Phys. Chem. C* 113, 3881–3886.
- Wu, H.-P., Ou, Z.-W., Pan, T.-Y., Lan, C.-M., Huang, W.-K., Lee, H.-W., Reddy, N.M., Chen, C.-T., Chao, W.-S., Yeh, C.-Y., Diau, E.W.-G., 2012. Molecular engineering of cocktail co-sensitization for efficient panchromatic porphyrin-sensitized solar cells. *Energy Environ. Sci.* 5, 9843.
- Wu, Y., Marszalek, M., Zakeeruddin, S.M., Zhang, Q., Tian, H., Grätzel, M., Zhu, W., 2012. High-conversion-efficiency organic dye-sensitized solar cells: molecular engineering on D–A– $\pi$ -A featured organic indoline dyes. *Energy Environ. Sci.* 5, 8261.
- Wu, Y., Zhu, W., 2013. Organic sensitizers from D– $\pi$ -A to D–A– $\pi$ -A: effect of the internal electron-withdrawing units on molecular absorption, energy levels and photovoltaic performances. *Chem. Soc. Rev.* 42, 2039–2058.
- Yang, J., Ganesan, P., Teuscher, J., Moehl, T., Kim, Y.J., Yi, C., Comte, P., Pei, K., Holcombe, T.W., Nazeeruddin, M.K., Hua, J., Zakeeruddin, S.M., Tian, H., Grätzel, M., 2014. Influence of the Donor Size in D– $\pi$ -A Organic Dyes for Dye-Sensitized Solar Cells. *J. Am. Chem. Soc.* 136, 5722–5730.
- Yao, Z., Zhang, M., Wu, H., Yang, L., Li, R., Wang, P., 2015. Donor/Acceptor Indenoperylene Dye for Highly Efficient Organic Dye-Sensitized Solar Cells. *J. Am. Chem. Soc.* 137, 3799–3802.
- Yeh-Yung Lin, R., Wu, F.-L., Chang, C.-H., Chou, H.-H., Chuang, T.-M., Chu, T.-C., Hsu, C.-Y., Chen, P.-W., Ho, K.-C., Lo, Y.-H., Lin, J.T., 2014. Y-shaped metal-free D– $\pi$ -(A)<sub>2</sub> sensitizers for high-performance dye-sensitized solar cells. *J. Mater. Chem. A* 2, 3092.
- Zhang, H., Fan, J., Iqbal, Z., Kuang, D.-B., Wang, L., Meier, H., Cao, D., 2013. Novel dithieno[3,2-b:2',3'-d]pyrrole-based organic dyes with high molar extinction coefficient for dye-sensitized solar cells. *Organic Electronics* 14, 2071–2081.
- Zhang, L., Cole, J.M., 2017. Dye aggregation in dye-sensitized solar cells. *J. Mater. Chem. A* 5, 19541–19559.
- Zhang, L., Cole, J.M., 2015. Anchoring Groups for Dye-Sensitized Solar Cells. *ACS Appl. Mater. Interfaces* 7, 3427–3455.
- Zhang, Z., Yates, J.T., 2012. Band Bending in Semiconductors: Chemical and Physical Consequences at Surfaces and Interfaces. *Chem. Rev.* 112, 5520–5551.